Stimulus induced strain in spin transition heterostructures ⊘

John M. Cain (ID) ; Wanhong He (ID) ; Isabelle Maurin ✉ (ID) ; Mark W. Meisel ✉ (ID) ; Daniel R. Talham ✉ (ID)

🔴 Check for updates

🌐 View Online ↱ Export Citation

Articles You May Be Interested In

High-entropy and compositionally complex battery materials

J. Appl. Phys. (March 2024)

On factors limiting the performance of photoelectrochemical CO_2 reduction

J. Chem. Phys. (March 2020)

Quasi-degenerate states and their dynamics in oxygen deficient reducible metal oxides

J. Chem. Phys. (February 2020)

Stimulus induced strain in spin transition heterostructures

John M. Cain,[1] Wanhong He,[1] Isabelle Maurin,[2,a)] Mark W. Meisel,[3,a)] and Daniel R. Talham[1,a)]

AFFILIATIONS

[1]Department of Chemistry, University of Florida, Gainesville, Florida 32611-7200, USA
[2]Physique de la Matière Condensée, UMR 7643, Ecole Polytechnique, CNRS, IP Paris, Palaiseau 91128, France
[3]Department of Physics and National High Magnetic Field Laboratory, University of Florida, Gainesville, Florida 32611-8440, USA

Note: This paper is part of the Special Topic on Spin Transition Materials: Molecular and Solid-State.
[a)]**Authors to whom correspondence should be addressed:** isabelle.maurin@polytechnique.edu, meisel@phys.ufl.edu,
and talham@chem.ufl.edu

ABSTRACT

Strain is often used to alter material properties in applications ranging from bandgap tuning for semiconductor electronics to performing work through mechanical actuation. Spin transitions are accompanied by volume changes in the solid state and are being explored in actuation as a source of mechanical strain inducible by the many controllable stimuli known to trigger spin state changes. There is still much to understand, especially at small length scales, about how strain is transmitted from one material to another across a mechanically coupled interface. Theoretical efforts modeling spin-transition particles in a matrix provide significant insights, but this remains an area where systematic experimental studies are limited. This Perspective highlights the progress using cobalt hexacyanoferrate network solids, or Prussian blue analogues (CoFe-PBA), as a framework for investigating spin transition induced strain in nanometer scale and mesoscale heterostructures. Using a family of isostructural cyanometallate networks to form heterostructures with well-defined interfaces, measurements of the altered properties in response to strain generated by the thermally or optically induced spin state change of the CoFe-PBA provide the chance to experimentally interrogate factors that control interface transmitted strain.

Published under license by AIP Publishing. https://doi.org/10.1063/5.0045939

I. INTRODUCTION

The defining characteristic of spin-transition materials[1,2] is the ability to change the total spin quantum number, S, in response to external stimuli such as temperature, light, pressure, or guest intercalation.[3–6] For magnetic applications, it is the change in spin state that is most useful, while switchable optical properties arise from the change in the spatial component of the ground-state wavefunction. Most spin-transition materials are transition metal complexes, and within the framework of ligand field theory this change in the orbital occupancy has structural consequences as electrons populate and depopulate metal-ligand π-bonding and σ-antibonding orbitals, effectively changing the bond order as the spin state is changed.[7] In the solid state, the additional interaction with the lattice gives rise to hysteresis in the spin transition, imparting bistability that has been the focus of much of the research into the optical and magnetic properties.

Often overlooked are the structural changes associated with the spin transition, which routinely produce changes in volume, often on the order of 5%–10% and sometimes greater.[8]

This relatively large change in volume has recently been exploited to drive novel mechanical actuators.[9–13] Shepherd *et al.*[13] devised bilayer actuators by coupling single crystals or polymer composites of spin-crossover materials to a non-switching layer. The different extents of expansion of the two layers during the spin transition cause spontaneous strain, leading to deflection of the bilayer cantilever and the potential for applications in wireless actuation. The concept was extended to demonstrate electromechanical actuators made of particles of the spin-crossover complex [Fe(Htrz)$_2$(trz)](BF$_4$) (Htrz = 1,2,4-4H-triazole and trz = 1,2,4-triazole) dispersed in a poly(methylmethacrylate) matrix.[11] Electrical energy is converted into mechanical motion through Joule heating of the spin-crossover/polymer composite in contact with an inert layer as part of a cantilever whose motion is controllable by modulating

the current.[12] Other examples taking advantage of this bimorph geometry to generate motion range from micrometer scale MEMS devices to centimeter scale "artificial muscles" performing work.[14] Related applications couple the volume change of the spin crossover (SCO) material to a strain-sensitive conductor or ferroelectric to demonstrate electrical bistability[15] and thermoelectric devices.[16]

Whether it is a single crystal coupled to a second material in a particle or on a surface, or nanocrystals embedded in a matrix, the spin-transition material in these actuators induces a deviatoric strain across a mechanically coupled interface. The magnitude and characteristics of the strain depend strongly on (1) the quality of the interface, (2) the actuator geometry, (3) the elastic properties of the material forming the matrix or substrate, and (4) the degree to which the spin transition is modified by the interfacial surface energy and feedback stresses into the spin-transition material. Early understanding of these issues is attributable to theoretical efforts to model spin-transition particles in a matrix or at an interface.[17–20] Still, this is an area where experimental systems are needed to elucidate the details, at chemical and nanomaterial length scales, of how spin-transition materials can propagate strain across an interface.

The cobalt hexacyanoferrate network solids provide a valuable platform for investigating spin transition induced strain, Fig. 1. Cubic Prussian blue analogues (PBAs) have the general formula $M_jA_k[B(CN)_6]_l \cdot nH_2O$ (abbreviated MAB-PBA or AB-PBA in this article) where A and B can be divalent or trivalent transition metals in ratios that depend on the relative charges of the metal ions and the number of charge-balancing cyanometallate vacancies or monovalent cations, M^+, in the structure. The CoFe-PBA spin transition is well studied[21–24] and nanometer scale or mesoscale (hundreds of nm to micrometers) particles can be readily prepared without

surface modifiers[25,26] enabling fabrication of core–shell[26–38] or thin film[39–41] heterostructures in which the spin-transition material interacts directly with a second component. Importantly, there are several isostructural PBAs that can be grown directly on the spin-transition solid, often epitaxially[26,27] and that are capable of accommodating strain, which can be quantified with structural analyses or alterations of physical properties.[27–41] In one of the more thoroughly studied architectures, the spin transition in the CoFe-PBA core alters the magnetization of a ferromagnetic nickel hexacyanochromate (NiCr-PBA) shell, Fig. 2. The uniform, relatively ideal interface in such heterostructures provides an important control when studying this complex problem.

II. SPIN-TRANSITION HETEROSTRUCTURES BASED ON CoFe-PBA

For a range of CoFe-PBA compositions, the cyanide bridged cobalt–iron pairs can exist as either Fe^{2+}-CN-$Co^{3+}_{(LS)}$ or Fe^{3+}-CN-$Co^{2+}_{(HS)}$ with the cobalt ion undergoing a spin-state change.[21–24] The spin transition causes a significant change in the Co–N bond length and is responsible for a dramatic change in lattice constant from below 10.0 Å in the low-spin (LS) phase to about 10.3 Å in the high-spin (HS) phase, Fig. 1.[37] The transition between these charge states can be either thermally or optically activated, with the thermal transition occurring slightly below room temperature, often with significant hysteresis due to strong electron-lattice coupling.[22–24] If the temperature is low enough, below about 150 K, the metastable high-spin state can also be optically accessed and trapped, as depicted in the scheme in Fig. 1. This optical process is directly analogous to the light-induced excited spin state trapping (LIESST)[1,42–45]
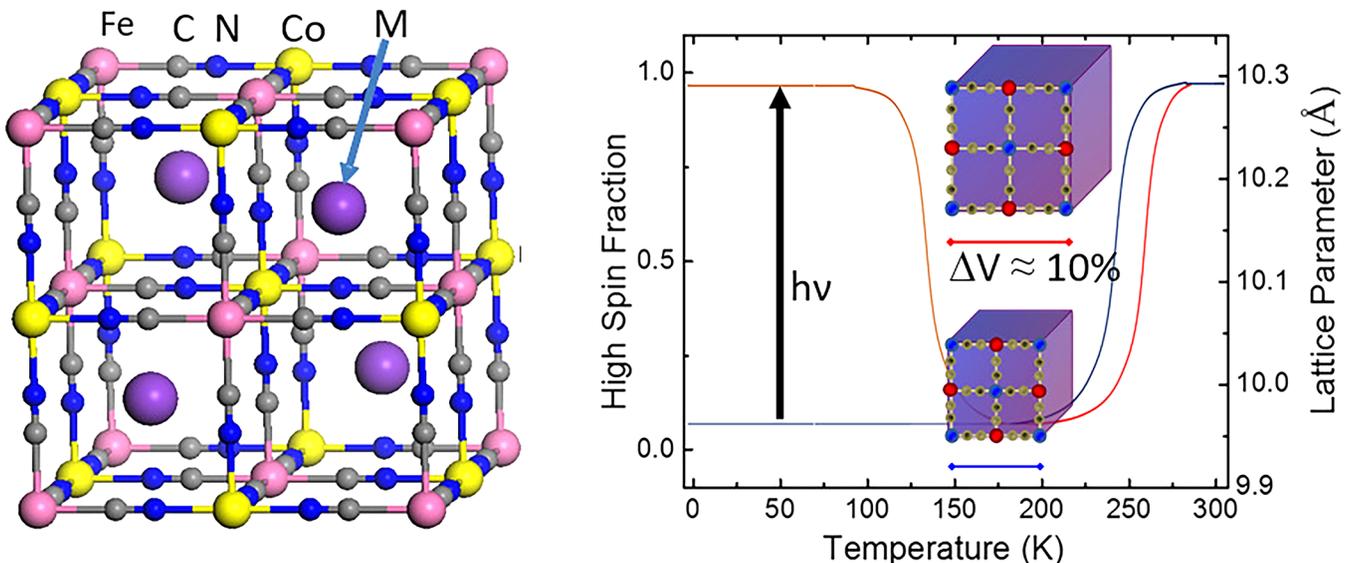
FIG. 1. (Left) The cubic structure of the cobalt hexacyanoferrate Prussian blue analogue (CoFe-PBA). Typically, a combination of cyanometallate vacancies and monovalent cations, M^+, are present to balance charge. (Right) Scheme depicting the structural changes accompanying both the thermal and light activated charge transfer coupled spin transition (CTCST) experienced by many CoFe-PBA compositions.
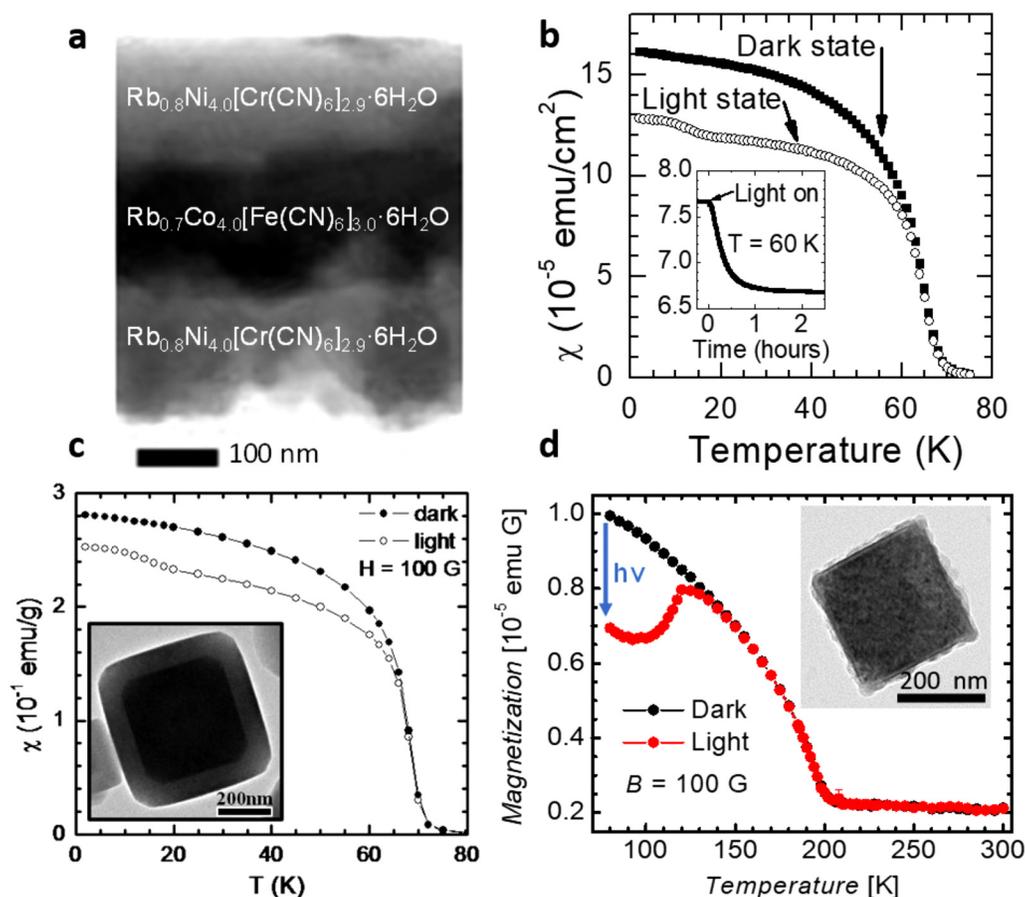
FIG. 2. (a) Heterostructure thin film sandwiching the CTCST compound RbCoFe-PBA with the ferromagnet RbNiCr-PBA.[39] (b) Magnetic susceptibility in the light and dark state for a thin film heterostructure similar to the one depicted in (a).[39] (c) Magnetic susceptibility in the light and dark states for a core–shell sample with RbCoFe-PBA core and KNiCr-PBA shell, showing similar behaviors for the thin film and mesoscale particle samples.[32] (d) Magnetization vs temperature in light and dark states for a RbCoFe-PBA@KCrCr-PBA core–shell sample showing photomagnetism above 100 K, up to the temperature where the metastable high-spin state of the core relaxes back to the low-spin state.[35] [Panels (a) and (b) adapted with permission from Pajerowski et al., J. Am. Chem. Soc. **132**, 4058–4059 (2010). Copyright 2010 American Chemical Society. Panel (c) adapted with permission from Dumont et al., Inorg. Chem. **50**, 4295–4300 (2011). Copyright 2011 American Chemical Society. Panel (d) adapted with permission from Risset et al., Chem. Mater. **27**, 6185–6188 (2015). Copyright 2015 American Chemical Society.]

transition seen in other spin-crossover materials. Since its discovery, the combined electron transfer/spin transition process is commonly referred to as a charge transfer induced spin transition (CTIST) throughout the literature, although the reality is closer to correlation than causation.[46] A very recent study of the optical process for nanocrystals of $Cs_{0.7}Co(Fe(CN)_6)_{0.9}$ clearly shows the Co-ion spin-crossover process occurring within 50 fs and preceding the charge transfer, which occurred on the 200 fs timescale.[47] It remains to be understood if the result also holds for the thermal process, or if the mechanism remains the same for all CoFe-PBA compositions. Nevertheless, this elegant finding shows that the continued use of the acronym CTIST, while correctly tying the phenomenon to the previous literature, is potentially incorrect and misleading. For the remainder of this article, we will use the acronym CTCST for charge transfer *coupled* spin

transition, while recognizing it is the same process referred to in other literature as CTIST.

Early examples of synergy between the spin transition in CoFe-PBA and another material were seen in thin film heterostructures of CoFe-PBA interfaced with nickel hexacyanochromate, NiCr-PBA, or cobalt hexacyanochromate, CoCr-PBA (Fig. 2). The NiCr-PBA and CoCr-PBA magnetically order ($T_C^{NiCr} \sim 70$ K, $T_C^{CoCr} \sim 30$ K) but do not exhibit native photomagnetic effects.[48,49] However, below their ordering temperatures, the light-induced CTCST of the CoFe-PBA network dramatically changes the magnetization of the NiCr-PBA or CoCr-PBA layers.[39,40]

Although these thin films are easy to fabricate, the interfaces are relatively rough and some studies are limited by the small amount of material. Both problems are circumvented by the readily available routes developed by Catala and co-workers[27,38] to well-defined

core–shell particles combining two or more isostructural PBA lattices. Core–shell heterostructures of several compositions have been developed, with particle sizes on the length scale studied in the thin film heterostructures, ~100 nm, and shells with thicknesses ranging from just a few nm to many tens of nm.[26–38]

As was reported for the thin film heterostructures, synergistic responses coupling the spin transition of the CoFe-PBA core with the magnetization of the magnetic but non-spin transition and optically inactive shell are observed. As shown in Fig. 2 for a CoFe-PBA@NiCr-PBA sample, the light-induced CTCST of the core causes a decrease in magnetization at temperatures up to the ordering temperature of the shell, ~70 K.[32,36,37] A similar result is observed with CoFe-PBA@CoCr-PBA with a CoCr-PBA ordering temperature of ~30 K.[33] Another combination, CoFe-PBA@CrCr-PBA core–shell particles, also shows a light-induced change in magnetization, but in this case the relationship to the spin transition of the core is directly seen in the magnetization vs temperature plot, Fig. 2.[35] The CrCr-PBA shell magnetically orders near 225 K,[50] but the light-induced change is only seen below ~150 K, the temperature above which the metastable HS state relaxes back to the ground state. The HS-LS transformation of the core is detected by the changing behavior of the shell.

The magnetization changes in the shell are attributable to structural distortions induced by mechanical stresses when the core lattice constant changes upon undergoing the spin transition.[33,36,37,51] Significant lattice contraction in the RbCoFe-PBA core upon cooling through the high-spin to low-spin transition near ~260 K induces a strained state of the shell PBA lattice. This strain can be relieved either by thermal cycling back to high temperature or by using light to access the metastable high-spin state of the core at low temperature. The light-induced change in magnetization is consistent with a realignment of the local magnetic anisotropy axes as a result of the structural changes in the shell. Since the spin transition temperature in the core is higher than the magnetic ordering temperature of the shell, the heterostructures are magnetized in the strained state. Relieving the strain reorients the preferred anisotropy axes causing magnetic moments originally aligned along the external field to shift away from the applied field, thereby reducing the measured bulk magnetization and giving the observed photoresponse.[52]

III. EVIDENCE OF STRAIN

Diffraction studies provide direct evidence for the elastic origin of the magnetization changes and for the development of significant strain in the PBA shells as a result of the spin transition of the CoFe-PBA core. The lattice contraction associated with the HS to LS transition can be monitored by powder x-ray diffraction, as shown for RbCoFe@KNiCr-PBA and RbCoFe@KCoCr-PBA examples in Fig. 3.[33] Shifts of the diffraction peaks corresponding to the shell lattices are observed in response to the contraction of the core when the sample is cooled from room temperature to below the spin transition temperature of the core. For the RbCoFe@KCoCr-PBA example with a 23 nm shell, the KCoCr-PBA lattice parameter contracts by 0.058 Å, from 10.551 to 10.493 Å, a relative strain of 0.55%. Similar results are reported for other shell compositions. For an RbCoFe@KNiCr-PBA sample with 14 nm shell, the shell

unit cell edge contraction is 0.081 Å.[36] In general, the change is largest for the thinnest shells, which provide the least resistance to the contraction of the core.

In contrast, the light-induced transition between the low-temperature LS state and the metastable HS state can also be used to build up strain in the shell,[29–31] instead of relieving it, when the RbCoFe-PBA particles are synthesized with a stoichiometry that results in the LS state configuration at room temperature. Core–shell particles prepared based on such CoFe-PBA cores can then be cooled to low temperature in the as-synthesized state. As a consequence, the light-induced CTCST from low spin to high spin will induce tensile stresses within the shell layer through the expansion of the core, as shown in Figs. 3(d) and 3(e). For one of these LS RbCoFe-PBA@KNiCr-PBA samples with an 11 nm shell, an *expansion* of the shell lattice by 0.08 Å was measured by PXRD, while for a RbCoFe-PBA@KNiFe-PBA sample the expansion is 0.09 Å.[29] It is interesting that for similar core and shell dimensions, the extent of shell expansion when the heterostructures prepared with a LS core transition from LS to HS is effectively the same as the extent of shell contraction when particles synthesized with a HS core transition from HS to LS.

An interesting example is provided by RbCoFe-PBA@KNiCo-PBA, prepared with the core in the HS state at room temperature. The equilibrium unit cell constant of the nickel hexacyanocobaltate, KNiCo-PBA, is 10.10 Å, smaller than for the HS RbCoFe-PBA yet larger than for the LS RbCoFe-PBA. So, unlike the other examples, as the core undergoes the spin transition, its cell constant changes from larger than that of the shell lattice to smaller. The result is a dramatic decrease of 0.17 Å for the shell lattice constant, corresponding to 1.7% strain, in a RbCoFe-PBA@KNiCo-PBA sample with a 7 nm shell. The shell lattice starts out slightly expanded as a result of growth on the larger lattice constant HS core, but ends up slightly compressed when the core transitions to the LS state. The magnitude of the change is nearly twice that of the other examples that only experience compressive stresses or only tensile stresses.

IV. ANALYSIS OF STRAIN

As already mentioned, the impact of the compressive or tensile forces exerted by the core particles on the shell can be qualitatively assessed by shifts of the Bragg reflections. A remaining challenge is to directly map the strain field within the shell layer in order to correlate the shell behavior with specific structural distortions. However, spatial resolution is currently greater than 5 nm using coherent x-ray diffractive imaging and these experiments are further complicated by dose tolerance in the case of molecular compounds that are prone to radiation damage when intense x-ray beams are focused on single objects. This reduced spatial resolution strongly hinders the investigation of the interface region where we expect the largest structural modifications.

Nevertheless, in many cases information on the strain field can still be obtained through the analysis of the diffraction line shapes, including peak width and peak asymmetry that are both representative of distributions of interspacing distances. For PBA core–shell heterostructures, direction-dependent line broadening is reported for as-grown shell lattices and is attributed, at least in part, to size effects and formation of platelet shell crystallites that
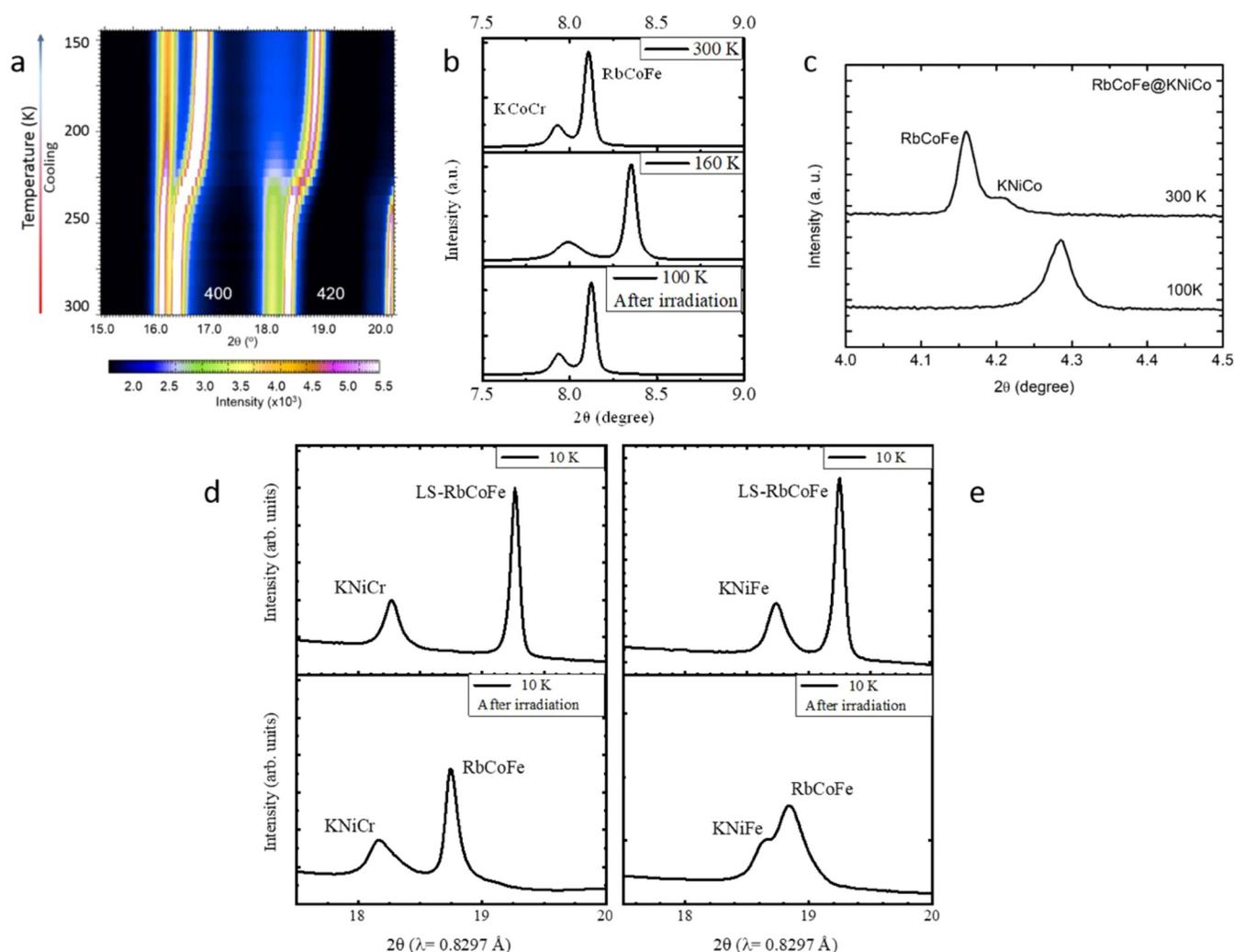
FIG. 3. Evidence of strain developed in core–shell particles following CTCST of the CoFe-PBA core. (a) PXRD vs temperature stack plot of a RbCoFe-PBA@KNiCr-PBA sample with 15 nm shell showing a shift and broadening of the (400) and (420) KNiCr-PBA peaks (left hand peaks in each doublet) accompanying the thermal spin transition in the RbCoFe-PBA core (right hand peaks in each pair).[37] (b) Partial PXRD patterns ($\lambda = 0.187\ 156$ Å) showing the (400) reflections of both components of a RbCoFe-PBA@KCoCr-PBA core–shell sample in the room temperature as-synthesized high-spin state, at 160 K after the core transitions to the low-spin state causing the (400) peak of the shell to shift and broaden, and at 100 K after the optical CTCST back to the high-spin state of the core relieving the strain.[33] (c) The (200) reflections of a RbCoFe-PBA@KNiCo-PBA sample with a 7 nm shell. The equilibrium lattice constant of the KNiCo-PBA is in between the lattice constants of the high-spin and low-spin core. [(d) and (e)] PXRD profiles of core–shell particle samples prepared with the RbCoFe core in the low-spin state, showing the shift and broadening of the corresponding (400) shell peaks after the optical transition of the core from low spin to high spin. [Panel (a) adapted with permission from Felts et al., J. Phys. Chem. C **120**, 5420–5429 (2016). Copyright 2016 American Chemical Society. Panel (b) adapted with permission from Risset et al., J. Am. Chem. Soc. **136**, 15660–15669 (2014). Copyright 2014 American Chemical Society.].

are parallel to the facets of the cubic cores. The (001) plane of shell lattices grow parallel to the (001) plane of RbCoFe-PBA core,[26] resulting in (hkl) peaks 20%–30% broader than the (h00) peaks for the thinnest shells.[31] However, additional sources of line broadening in these core–shell structures are a result of the epitaxial growth of mismatched lattices. The equilibrium lattice constant of the CoFe-PBAs is near 10.3 Å in the HS state and near 10.0 Å in the

LS state, shifting some as exact compositions vary. The isostructural shell cyanometallates can range from below 10.0 Å to greater than 10.5 Å for different analogues, so different core–shell combinations will exhibit different extents of line broadening as-grown. The different contributions to peak broadening can be quantified[29,33,36] through Williamson–Hall plot analyses that deconvolute size reduction and local strain effects by taking advantage of their different

scattering angle dependences,[53–55]

$$\frac{H \cos \theta}{\lambda} = \varepsilon \frac{2 \sin \theta}{\lambda} + \frac{1}{L_c},$$ (1)

where H refers to the full width at half-maximum corrected for the instrument resolution function, θ is the angle of diffraction, λ refers to the wavelength of the incident x rays, L_c represents the apparent size along a given [hkl] direction, and ε quantifies the local strain (also called microstrain). When plotted, Eq. (1) yields the structural coherence length as the intercept and non-uniform strain contributions as the slope.

For spin-transition heterostructures, Williamson–Hall analyses have revealed the development of anisotropic microstrain, with different magnitudes along the [h00] and other [hkl] directions, suggesting non-uniform strain fields in the shell layers.[29,33,36] For instance, the difference in equilibrium lattice constants between the core and the shell when the KNiCr-PBA shell is grown on high-spin CoFe-PBA core particles is $\Delta a \sim 0.16$ Å. In that case, prior to the thermal HS to LS transition, the ε-value derived from the (hkl) peaks is $0.40\% \pm 0.01\%$. As the sample temperature is lowered through the RbCoFe-PBA thermal CTCST, the change in KNiCr-PBA peak positions is indicative of a global contraction of the lattice by 0.77% for a sample with a 160 nm core and a 15 nm shell. The microstrain parameter, ε, then increases from 0.4% for the KNiCr-PBA (hkl) reflections at 300 K to 3.2% at 100 K. The slight anisotropy of the broadening already present at room temperature is much more pronounced at 100 K.[36] Figure 4(a) shows similar behavior for a comparable thickness shell on a slightly smaller core particle.

An alternative approach to quantify anisotropic microstrain is to incorporate its contribution to the linewidth into the whole pattern refinement process, using the phenomenological model proposed by Stephens.[56] For the cubic PBA lattices, two parameters describe the generalized microstrain, S_{400} and S_{220}. The S_{400} parameter contributes to (h00) reflections while both contribute to (hkl) reflections. As with the Williamson–Hall analysis, it can be seen that anisotropic strain is imparted into the shell below the HS to LS phase transition temperature of the core. Similar behavior is seen for KCoCr-PBA shells grown on HS RbCoFe-PBA. As the core undergoes the thermal HS to LS transition, anisotropic microstrain again develops in the shell, with the (hkl) reflections exhibiting more microstrain than the (h00) reflections. In Fig. 4(b), S_{400} is used to monitor the build-up or release of strain in three different shell materials.

The as-grown KNiCr-PBA shell lattice experiences a higher degree of strain when formed on low-spin CoFe-PBA core particles, with an equilibrium difference in lattice parameter, Δa, of 0.55 Å. In that case, prior to the LS to HS transition, ε-values derived from the (hkl) peaks $(1.1\% \pm 0.2\%)$ are found to be five to six times larger than those related to the (h00) reflections. These direction-dependent ε-parameters can be attributed to internal stresses due to the epitaxial growth, likely reflecting the formation of misfit dislocations at the core/shell interface along with threading dislocations in the volume of the shell layer.[31] Figure 4(c) illustrates the impact of the mismatch between the core and shell lattices with an ε-parameter associated with the non-[h00] directions that increases
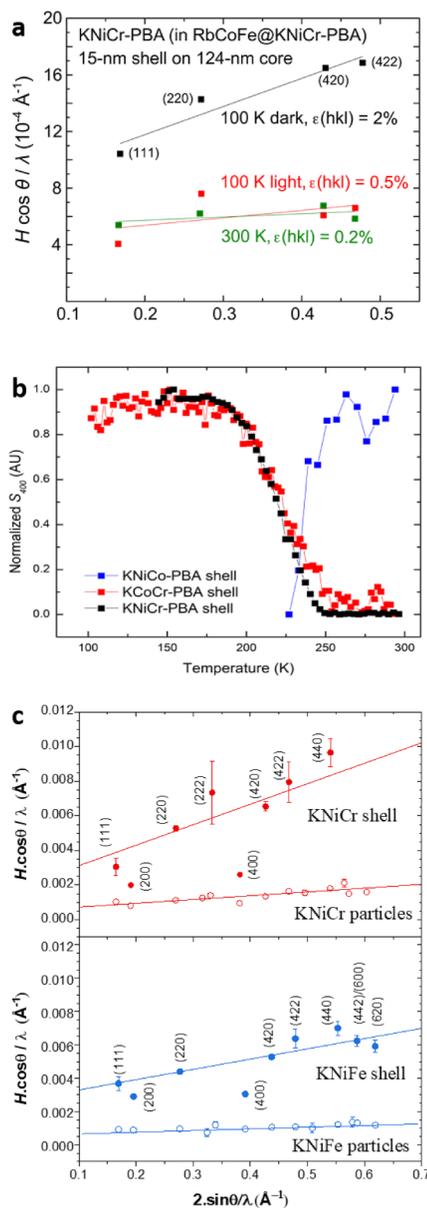
FIG. 4. (a) Williamson–Hall analysis of microstrain in the shell of an RbCoFe-PBA@KNiCr-PBA sample as-synthesized (300 K), after cooling below the thermal CTCST (100 K, dark) and after photoconversion to the metastable HS state of the core (100 K, light). The microstrain is largest after the spin transition, but relatively small in both the as-synthesized and 100 K light states. (b) Generalized microstrain parameter S_{400} for three different shell materials during the thermal HS-LS CTCST of the RbCoFe-PBA core. The equilibrium lattice constants of the KNiCr-PBA and KCoCr-PBA shells are close to that of the HS RbCoFe-PBA core, so microstrain increases during the HS–LS transition. On the other hand, microstrain in the as-synthesized KNiCo-PBA shell, with an equilibrium lattice constant smaller than the HS core, is reduced during the HS–LS transition. (c) Williamson–Hall plots showing microstrain of KNiCr-PBA and KNiFe-PBA shells when grown on LS CoFe-PBA core particles. Single phase controls are shown for comparison.

from 0.6% to 1.2% when the misfit increases from 2.6% to 5.3%. It is worth noting that similar findings were also reported for other PBA heterostructures without CoFe-PBA as the core.[34] Interestingly, in the LS RbCoFe-PBA@KNiCr-PBA particles, the lattice constant of the shell, which is similar to its equilibrium value before light irradiation, increases to larger than its equilibrium value after the light-induced LS to HS transition of the core. Contrary to the situation previously described, the light-induced CTCST mostly induces tensile stresses instead of leading to the relief of compressive forces, but the two situations both lead to significant structural disorder, with distributions of the interspacing distances of the order of several percent.

Given clear signatures of changing strain in the shell in response to the spin transition of the core, we can ask, "how much of the shell experiences the strain? What is the "strain depth" in the shell and how does it change with the dimensions of the spin transition core?" Magnetometry provides a route to isolate the contributions attributable to the strained shell by taking advantage of the ability to switch between the strained and unstrained conditions.[33,57] A model was developed that divides the magnetic response into three components: the core, the strained region of the shell, and the rest of the shell or bulk region beyond the influence of the transitioning core, Fig. 5. When the core undergoes the spin transition, the change in magnetization is composed of contributions from the core plus only the strained region of the shell, which can be isolated by subtracting the measured photoresponse of the uncoated core. Any uncertainty associated with this approach is greatly diminished by performing the analysis over a temperature range where the shell is ferromagnetic while the core is paramagnetic, so it contributes significantly less to the measurement. This treatment allowed for a sensitive determination of the strained region volume for a given core size by measuring a series of particles with successively thicker shells. The strained volume, and by extension strained thickness, was obtained by fitting the effective dilution of the photoactive strained region as unstrained and non-photoactive bulk-like material is added when the shell is made thicker.[57]

Three different RbCoFe-PBA core particle sizes were studied (124, 325, and 544 nm), Fig. 5. As expected, the maximum strain depth increases as the spin transition core particle becomes larger. More surprising is the magnitude of the strain depth. The magnetization of the KNiCr-PBA shell can be affected by interfacial strain to a depth of 110 nm for the 544 nm core example.[57] Such a significant distance from the interface is attributable to the flexibility of the KNiCr-PBA shell and the strength of the interfacial coupling. For thin shells, that is with shell thickness less than the strain depth, the volume change in the core becomes dependent on the thickness of the shell, with the largest shell strain for the thinnest shells, decreasing as the shell approaches the limiting strained
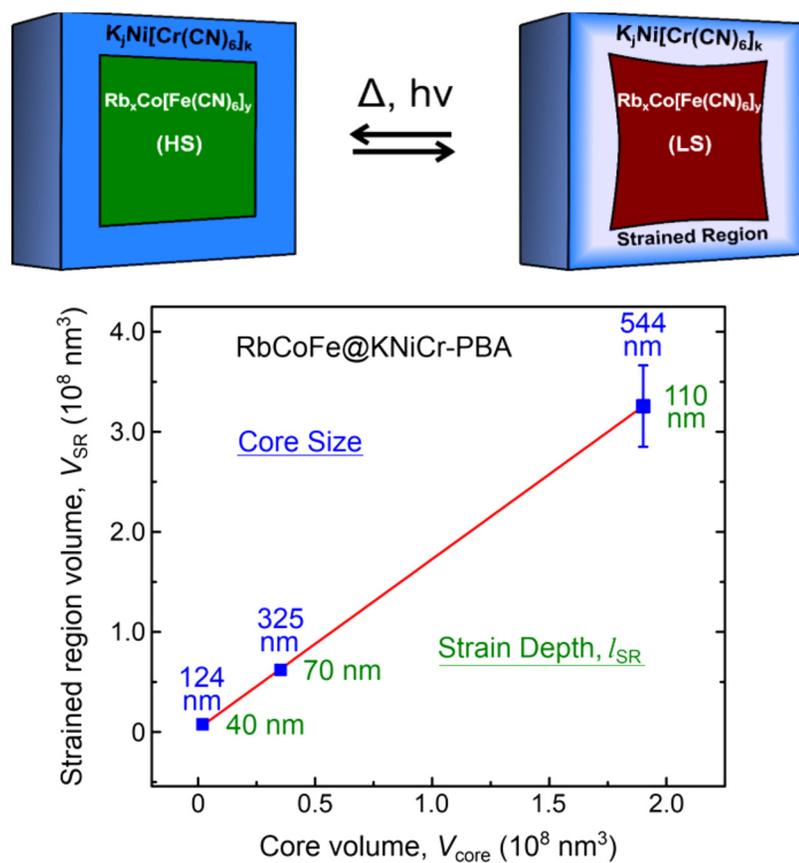
FIG. 5. Evaluation of the depth of the shell strained region following CTCST of the core in RbCoFe-PBA@KNiCr-PBA particles with differing core sizes. [Adapted with permission from Cain *et al.*, Chem. Mater. **33**, 246–255 (2021). Copyright 2021 American Chemical Society.]

region thickness. The nonlinear response in this region is a consequence of feedback between the shell and the actuating core.

V. REVIEW OF THE FACTORS THAT INFLUENCE STRAIN AND WHERE WE STAND TO PROBE THEM EXPERIMENTALLY

It was already stated that the magnitude and character of the strain in spin-transition heterostructures depend strongly on a series of factors: the quality of the interface, the elastic properties of the materials forming the heterostructures, the actuator geometry, and the degree to which the character of the spin transition is modified by the interfacial surface energy and any feedback stresses from the substrate. One of the motivations for using the PBA nanoparticle platform to explore the heterostructure strain is the high quality of the interface between PBA components. With isostructural lattices, epitaxy between core and shell has been confirmed in some cases,[26,27,31] we can assume a near ideal interface and consider it effectively as a constant when comparing different compositions, allowing the other factors related to material properties and particle geometry to be explored experimentally. We now address each of these factors, reflecting on how they are manifested in experimental studies of PBA heterostructures and relating the experimental results to current theoretical treatments.

Since the principal source of the strain in the shell comes from the volume change in the core, the most important considerations for strain engineering are the elastic properties of the actuator and of the matrix or substrate. For core–shell PBA heterostructures, the RbCoFe-PBA core plays the role of the actuator and the shell is the "matrix" in which it is suspended. Within continuum elastic models of defects in continuous solids, the core after undergoing its spin transition can be described as a "volume-misfit" defect in the lattice of the shell, since if the core and shell could somehow be separated and allowed to relax, the volume of the core would not match the volume of the cavity in the shell.[20,58–60] Eshelby found that for relatively small distortions, there is a proportionality constant, γ, between the volume misfit of the defect, ΔV_{defect}, and the total change in volume for the particle, $\Delta V_{crystal}$,

$$\Delta V_{crystal} = \gamma \cdot \Delta V_{defect}. \quad (2)$$

For a defect in a single-phase material, γ is dependent on both the bulk and shear modulus,

$$\gamma = \frac{3K + 4\mu}{3K}, \quad (3)$$

where K is the bulk modulus and μ is the shear modulus for the material.[58] Relating this description to the core–shell case, the contraction (or expansion) of the core involves not just a change in the volume of the core relative to the volume of the cavity, but also shearing in the plane of the core–shell interface. For core–shell systems, Eq. (3) has to be modified to account for the differences in elastic parameters of the shell and the core; however, the linear relationship between $\Delta V_{crystal}$ and ΔV_{defect} is maintained. This linearity has been shown to break down when the size of the core or shell becomes small enough to make the discrete nature of the lattice

important, and on these length scales γ becomes a function of particle size.[59] The excellent linear fit of the strained region volume, V_{SR}, with respect to core volume, V_{core}, in Fig. 5 shows that for RbCoFe@KNiCr-PBA particles with shell thicknesses thicker than 30 nm (and core sizes > 120 nm), the continuum approximation is appropriate, providing the advantage of well-defined analytical expressions that can be used to guide future experimental work.

Felix et al.[20] adapted the "volume-misfit" concept to develop a model conceptually similar to our particles, using a spin-transition core surrounded by an inert shell, which can be directly compared to the experimental results from studies of the PBA heterostructures. For sufficiently thick shells, the model predicts the elastic energy density for the core plateaus, and additional shell material has no effect on the elastic state of the core, implying the existence of a "strain depth" in the shell, beyond which any strain-induced effects are undetectable. This strain depth has been observed experimentally in both the RbCoFe@KNiCr-PBA and RbCoFe@KCoCr-PBA heterostructure systems using magnetometry (Fig. 5).[33,36] Furthermore, for shell thicknesses less than this strain depth the model predicts the elastic energy density of the shell becomes larger as the shell thickness becomes smaller, and this result is also observed experimentally, both as larger shifts in lattice constants and greater levels of microstrain. With increasing shell thickness, up to the strain depth, the energy density of the shell decreases. In response, the energy density of the core increases, a direct result of the increased stiffness of the shell forcing the core to accommodate a greater fraction of the elastic energy.[61] Although not featured in this Perspective, which is primarily focused on strain induced in the shell, these effects have also been observed experimentally. The RbCoFe-PBA core contracts to a reduced degree upon cooling when a shell is deposited on the surface,[33,36,37] decreasing further as the shell thickness increases, a direct reflection of this shifting elastic energy density. A consequence is a nonlinear dependence of the strain on shell thickness,[57] meaning that measurements of thin-shell core–shell samples cannot be used to map the strain profile present in the thick-shell analogues, but also that relatively small changes to the heterostructure geometry can change the strain profile substantially.

The importance of the actuator geometry can be clearly seen in the dramatic dependence of the shell strain on shell thickness for the thin-shell samples. In the cubic particle geometry, each face can be represented as a thin plate supported at its edges. As the core contracts, a force is applied to the plate, formally attributable to the image pressure. For a particle with spherical symmetry, this image pressure is a constant, but for other particle geometries the image pressure varies spatially.[58,59] The result in cubic particles is a bending of the shell, which has been seen in Monte Carlo simulations performed on square core–shell lattices (Fig. 6).[62]

The resistance of the "plate" to this flexure is referred to as the flexural rigidity and is proportional to t^3, where t is the plate thickness.[61] The importance of the particle geometry in the thin-shell regime cannot be overstated: while flexure is the primary mode of accommodating stress in a thin cubic shell, stretching is predicted to be the principal mode of stress accommodation for a thin spherical shell.

The strong agreement between experiment and theory when using the PBA heterostructure model is particularly promising, demonstrating its choice is valid for experimentally studying these

FIG. 6. Results of Monte–Carlo simulations on 2D core–shell particles after allowing a HS core particle to relax to the core LS state equilibrium LS.[61] The shell is seen to be undistorted when the equilibrium lattice parameters for the core and shell (R_c and R_s) are the same as in the initially prepared isometric lattices, but when these equilibrium lattice parameters are different, the strain is partially accommodated by distorting the particle. Adapted with permission from Affes et al., Chem. Phys. Lett. **718**, 46–53 (2019). Copyright 2019 Elsevier.

problems while providing confidence the strain generated by spin-transition actuators can be extensively tuned through thoughtful choices of components. Despite progress, opportunities remain for further fundamental studies.

VI. CONCLUDING COMMENTS AND SOME REMAINING QUESTIONS

As was emphasized above, particle geometry is particularly important. Experimentally, both cubic and spherical RbCoFe@KNiCr-PBA particles have been studied and significant differences have been observed, although variations in the particle sizes and in the RbCoFe-PBA core compositions used in these studies preclude definitive comparisons.[31,36,57] A more deliberate study of the effects of particle shape might allow a greater understanding of the roles that the core and shell geometry play in susceptibility to different types of strain.

There are also questions about how behavior changes at different length scales. Much of the work discussed here involves meso-scale particles, meaning dimensions on the order of ∼100 nm or more. Continuum mechanics has proven to be an effective framework, yet it is not obvious where the cutoff is. As systems get smaller, it will be important to determine at what point continuum mechanics begin to break down, when atomistic approaches are most appropriate, and whether these length scales change with varying particle geometries. This latter possibility seems likely given the shape-dependent scaling behavior of the elastic properties seen in simulations.[18] Line and planar defects such as dislocations or grain boundaries may also impact the mechanical response of the shell or the transformation process of the core itself.

Related questions surround the non-uniform strain field produced by the spin transition. Corners of cubic particles should experience weaker coupling to the core than the faces providing an additional source of anisotropy, but also a strain gradient parallel to the face. At the same time, for thicker shells a strain gradient is seen normal to the cubic faces. The very strong (400) peak asymmetry reported in Fig. 3(d) for the LS RbCoFe-PBA@KNiCr-PBA heterostructure is suggestive of crystallographic directions that are in compression after light irradiation as well as directions in expansion, leading to the possibility of local structural changes in the shell, at least close to the interface.

The fundamental limitation on tuning the strain profile in spin-transition heterostructures, of course, is the sensitivity of the spin transition itself to the elastic properties of the lattice.[17,63–65] The increased strain present in the core for thick-shell heterostructures has been predicted to result in a residual HS fraction in the core (when contracting against a stiff shell), softening the LS lattice. The presence of an incomplete spin transition is expected to substantially modify the strain transmitted across the interface, since both the image pressure and the elastic properties of the core matrix are modified. At the same time, the microscopic transformation process of the core itself can have an influence on how strain is induced. Numerical simulations predict the presence of a shell can change how the spin transition propagates, for example, proceeding heterogeneously through the nucleation and growth of domains in uncoated or thin shell particles while thicker shells lead to a homogeneous or statistical process.[17] The dissipation of strain in the shell may not be the same with these different mechanisms in the core. The temperature difference between the thermal CTCST processes and where the light-induced CTCST is observed may also lead to stimulus-dependent pathways for dissipating the strain. The strain field developed during a thermal process may be only partly relaxed at the cryogenic temperatures used for photo-excitation. Certainly, there are opportunities for further detailed explorations of the interplay between the actuating core and the stress responsive shell.

03 March 2026 20:53:14

DATA AVAILABILITY

The data that support the findings of this study are available from the corresponding authors upon reasonable request.

REFERENCES

[1]P. Gutlich, A. Hauser, and H. Spiering, Angew. Chem. Int. Ed. Eng. **33**, 2024 (1994).

[2]P. Gutlich, Y. Garcia, and H. A. Goodwin, Chem. Soc. Rev. **29**, 419 (2000).

[3]A. Bhattacharjee, V. Ksenofontov, H. Goodwin, and P. Gutlich, J. Phys.: Condens. Matter **21**, 026011 (2009).

[4]I. Boldog, A. Gaspar, V. Martinez, P. Pardo-Ibanez, V. Ksenofontov, A. Bhattacharjee, P. Gutlich, and J. Real, Angew. Chem. Int. Ed. Eng. **47**, 6433 (2008).

[5]S. Bedoui, M. Lopes, W. Nicolazzi, S. Bonnet, S. Zheng, G. Molnár, and A. Bousseksou, Phys. Rev. Lett. **109**, 135702 (2012).

[6]M. Ohba, K. Yoneda, G. Agusti, M. Munoz, A. Gaspar, J. Real, M. Yamasaki, H. Ando, Y. Nakao, S. Sakaki, and S. Kitagawa, Angew. Chem. Int. Ed. Eng. **48**, 4767 (2009).

[7]A. Hauser, P. Gutlich, and H. Goodwin, "Spin crossover in transition metal compounds I," Top. Curr. Chem. **233**, 49 (2004).

[8]P. Guionneau, Dalton Trans. **43**, 382 (2014).

[9]B. Kundys, Appl. Phys. Rev. **2**, 011301 (2015).

[10]M. D. Manrique-Juarez, S. Rat, L. Salmon, G. Molnar, C. M. Quintero, L. Nicu, H. J. Shepherd, and A. Bousseksou, Coord. Chem. Rev. **308**, 395 (2016).

[11]M. D. Manrique-Juarez, F. Mathieu, V. Shalabaeva, J. Cacheux, S. Rat, L. Nicu, T. Leichle, L. Salmon, G. Molnar, and A. Bousseksou, Angew. Chem. Int. Ed. Eng. **56**, 8074 (2017).

[12]I. A. Gural'skiy, C. M. Quintero, J. S. Costa, P. Demont, G. Molnar, L. Salmon, H. J. Shepherd, and A. Bousseksou, J. Mater. Chem. C **2**, 2949 (2014).

[13]H. J. Shepherd, I. A. Gural'skiy, C. M. Quintero, S. Tricard, L. Salmon, G. Molnar, and A. Bousseksou, Nat. Commun. **4**, 9 (2013).

[14]M. D. Manrique-Juarez, F. Mathieu, A. Laborde, S. Rat, V. Shalabaeva, P. Demont, O. Thomas, L. Salmon, T. Leichle, L. Nicu, G. Molnar, and A. Bousseksou, Adv. Funct. Mater. **28**, 1801979 (2018).

[15]Y. C. Chen, Y. Meng, Z. P. Ni, and M. L. Tong, J. Mater. Chem. C **3**, 945 (2015).

[16]M. Piedrahita-Bello, B. Martin, L. Salmon, G. Molnar, P. Demont, and A. Bousseksou, J. Mater. Chem. C **8**, 6042 (2020).

[17]H. Oubouchou, A. Slimani, and K. Boukheddaden, Phys. Rev. B **87**, 104104 (2013).

[18]A. Slimani, K. Boukheddaden, and K. Yamashita, Phys. Rev. B **89**, 214109 (2014).

[19]A. Slimani and K. Boukheddaden, Phys. Chem. Chem. Phys. **20**, 28583 (2018).

[20]G. Felix, M. Mikolasek, G. Molnar, W. Nicolazzi, and A. Bousseksou, Eur. J. Inorg. Chem. **2018**, 435.

[21]O. Sato, T. Iyoda, A. Fujishima, and K. Hashimoto, Science **272**, 704 (1996).

[22]N. Shimamoto, S. Ohkoshi, O. Sato, and K. Hashimoto, Inorg. Chem. **41**, 678 (2002).

[23]A. Bleuzen, C. Lomenech, V. Escax, F. Villain, F. Varret, C. Cartier dit Moulin, and M. Verdaguer, J. Am. Chem. Soc. **122**, 6648 (2000).

[24]C. Moulin, F. Villain, A. Bleuzen, M. Arrio, P. Sainctavit, C. Lomenech, V. Escax, F. Baudelet, E. Dartyge, J. Gallet, and M. Verdaguer, J. Am. Chem. Soc. **122**, 6653 (2000).

[25]D. Brinzei, L. Catala, N. Louvain, G. Rogez, O. Stephan, A. Gloter, and T. Mallah, J. Mater. Chem. C **16**, 2593 (2006).

[26]L. Catala and T. Mallah, Coord. Chem. Rev. **346**, 32 (2017).

[27]L. Catala, D. Brinzei, Y. Prado, A. Gloter, O. Stephan, G. Rogez, and T. Mallah, Angew. Chem. Int. Ed. Eng. **48**, 183 (2009).

[28]N. Dia, L. Lisnard, Y. Prado, A. Gloter, O. Stephan, F. Brisset, H. Hafez, Z. Saad, C. Mathoniere, L. Catala, and T. Mallah, Inorg. Chem. **52**, 10264 (2013).

[29]A. Adam, M. Poggi, E. Larquet, R. Cortès, L. Martinelli, P. E. Coulon, E. Lahera, O. Proux, D. Chernyshov, K. Boukheddaden, T. Gacoin, and I. Maurin, Nanoscale **10**, 16030 (2018).

[30]M. Presle, J. Lemainque, J. Guigner, E. Larquet, I. Maurin, J. Boilot, and T. Gacoin, New J. Chem. **35**, 1296 (2011).

[31]M. Presle, I. Maurin, F. Maroun, R. Cortes, L. L. Lu, R. S. Hassan, E. Larquet, J. M. Guigner, E. Riviere, J. P. Wright, J. P. Boilot, and T. Gacoin, J. Phys. Chem. C **118**, 13186 (2014).

[32]M. F. Dumont, E. S. Knowles, A. Guiet, D. M. Pajerowski, A. Gomez, S. W. Kycia, M. W. Meisel, and D. R. Talham, Inorg. Chem. **50**, 4295 (2011).

[33]O. N. Risset, P. A. Quintero, T. V. Brinzari, M. J. Andrus, M. W. Lufaso, M. W. Meisel, and D. R. Talham, J. Am. Chem. Soc. **136**, 15660 (2014).

[34]O. Risset and D. Talham, Chem. Mater. **27**, 3838 (2015).

[35]O. Risset, T. Brinzari, M. Meisel, and D. Talham, Chem. Mater. **27**, 6185 (2015).

[36]A. Felts, M. Andrus, E. Knowles, P. Quintero, A. Ahir, O. Risset, C. Li, I. Maurin, G. Halder, K. Abboud, M. Meisel, and D. Talham, J. Phys. Chem. C **120**, 5420 (2016).

[37]A. Felts, A. Slimani, J. Cain, M. Andrus, A. Ahir, K. Abboud, M. Meisel, K. Boukheddaden, and D. Talham, J. Am. Chem. Soc. **140**, 5814 (2018).

[38]L. Catala, F. Volatron, D. Brinzei, and T. Mallah, Inorg. Chem. **48**, 3360 (2009).

[39]D. M. Pajerowski, M. J. Andrus, J. E. Gardner, E. S. Knowles, M. W. Meisel, and D. R. Talham, J. Am. Chem. Soc. **132**, 4058 (2010).

[40]D. M. Pajerowski, J. E. Gardner, F. A. Frye, M. J. Andrus, M. F. Dumont, E. S. Knowles, M. W. Meisel, and D. R. Talham, Chem. Mater. **23**, 3045 (2011).

[41]D. Talham and M. Meisel, Chem. Soc. Rev. **40**, 3356 (2011).

[42]C. Mathoniere, Eur. J. Inorg. Chem. **2018**, 248.

[43]M. Cammarata, S. Zerdane, L. Balducci, G. Azzolina, S. Mazerat, C. Exertier, M. Trabuco, M. Levantino, R. Alonso-Mori, J. Glownia, S. Song, L. Catala, T. Mallah, S. Matar, and E. Collet, Nat. Chem. **13**, 10 (2021).

[44]S. Decurtins, P. Gutlich, C. Kohler, H. Spiering, and A. Hauser, Chem. Phys. Lett. **105**, 1 (1984).

[45]J. Mcgarvey and I. Lawthers, J. Chem. Soc. Chem. Commun. **1982**, 906 (1982).

[46]A. Hauser, Chem. Phys. Lett. **124**, 543 (1986).

[47]J. F. Letard, J. Mater. Chem. **16**, 2550 (2006).

[48]V. Gadet, T. Mallah, I. Castro, M. Verdaguer, and P. Veillet, J. Am. Chem. Soc. **114**, 9213 (1992).

[49]S. Ohkoshi and K. Hashimoto, Chem. Phys. Lett. **314**, 210 (1999).

[50]T. Mallah, S. Thiebaut, and M. Verdaguer, and P. Veillet, Science **262**, 1554 (1993).

[51]D. Pajerowski, B. Ravel, C. Li, M. Dumont, and D. Talham, Chem. Mater. **26**, 2586 (2014).

[52]C. R. Gros, M. K. Peprah, B. D. Hosterman, T. V. Brinzari, P. A. Quintero, M. Sendova, M. W. Meisel, and D. R. Talham, J. Am. Chem. Soc. **136**, 9846 (2014).

[53]P. Scardi, M. Leoni, and R. Delhez, J. Appl. Crystallogr. **37**, 381 (2004).

[54]J. vanBerkum, R. Delhez, T. deKeijser, and E. Mittemeijer, Acta Crystallogr. A **52**, 730 (1996).

[55]G. Williamson and W. Hall, Acta Metall. **1**, 22 (1953).

[56]P. Stephens, J. Appl. Crystallogr. **32**, 281 (1999).

03 March 2026 20:53:14

[57]J. M. Cain, A. Felts, C. M, W. Meisel, and D. R. Talham, Chem. Mater. **33**, 246 (2021).

[58]J. D. Eshelby, in *Solid State Physics*, edited by F. Seitz and D. Turnbull (Academic Press, 1956), Vol. 3, p. 79.

[59]K. Boukheddaden, Phys. Rev. B **88**, 134105 (2013).

[60]N. Willenbacher and H. Spiering, J. Phys. C **21**, 1423 (1988).

[61]L. D. Landau, L. P. Pitaevskii, A. M. Kosevich, and E. M. Lifšic, *Theory of Elasticity*, 3rd ed. (Elsevier, Amsterdam, 2012).

[62]K. Affes, A. Slimani, A. Maalej, and K. Boukheddaden, Chem. Phys. Lett. **718**, 46 (2019).

[63]H. Spiering, K. Boukheddaden, J. Linares, and F. Varret, Phys. Rev. B **70**, 184106 (2004).

[64]A. Slimani, K. Boukheddaden, and K. Yamashita, Phys. Rev. B **92**, 014111 (2015).

[65]M. Mikolasek, G. Felix, H. Peng, S. Rat, F. Terki, A. I. Chumakov, L. Salmon, G. Molnar, W. Nicolazzi, and A. Bousseksou, Phys. Rev. B **96**, 035426 (2017).